Lung Registration using Automatically Detected Landmarks

T. Polzin, Institute of Mathematics and Image Computing, University of Lübeck

J. Rühaak, Fraunhofer MEVIS Project Group Image Registration, Lübeck

R. Werner, Department of Computational Neuroscience, University Medical Center Hamburg-Eppendorf

H. Handels, Institute of Medical Informatics, University of Lübeck

J. Modersitzki, Institute of Mathematics and Image Computing, University of Lübeck

Corresponding author: Thomas Polzin (e-mail: polzin@mic.uni-luebeck.de, phone: +49 451 3101-6115, fax: +49 451 3101-6104, address: Institute of Mathematics and Image Computing, Maria-Goeppert-Straße 3, Lübeck, Germany)

Summary

Objectives: Accurate registration of lung CT images is inevitable for numerous clinical applications. Usually, nonlinear intensity-based methods are used. Their accuracy is typically evaluated using corresponding anatomical points (landmarks; e.g. bifurcations of bronchial and vessel trees) annotated by medical experts in the images to register. As image registration can be interpreted as correspondence finding problem, these corresponding landmarks can also be used in feature-based registration techniques. Recently, approaches for automated identification of such landmark correspondences in lung CT images have been presented. In this work, a novel combination of variational nonlinear intensity-based registration with an approach for automated landmark correspondence detection in lung CT pairs is presented and evaluated.

Methods: The main blocks of the proposed hybrid intensity- and feature-based registration scheme are a two-step landmark correspondence detection and the so-called CoLD (Combining Landmarks and Distance Measures) framework. The landmark correspondence identification starts with feature detection in one image followed by a block-matching-based transfer of the features to the other image. The established correspondences are used to compute a thin-plate spline (TPS) transformation. Within CoLD, the TPS transformation is improved by minimization of an objective function consisting of a Normalized Gradient Field distance measure and a curvature regularizer; the landmark correspondences are guaranteed to be preserved by optimization on the kernel of the discretized landmark constraints.

Results: Based on ten publicly available end-inspiration/expiration CT scan pairs with anatomical landmark sets annotated by medical experts from the DIR-Lab database, it is shown that the hybrid registration approach is superior in terms of accuracy: The mean distance of expert landmarks is decreased from 8.46 mm before to 1.15 mm after registration, outperforming both the TPS transformation (1.68 mm) and a nonlinear registration without usage of automatically detected landmarks (2.44 mm). The improvement is statistically significant in eight of ten datasets in comparison to TPS and in nine of ten datasets in comparison to the intensity-based registration. Furthermore, CoLD globally estimates the breathing-induced lung volume change well and results in smooth and physiologically plausible motion fields of the lungs.

Conclusions: We demonstrated that our novel landmark-based registration pipeline outperforms both TPS and the underlying nonlinear intensity-based registration without landmark usage. This highlights the potential of automatic landmark correspondence detection for improvement of lung CT registration accuracy.

Keywords: Lung; Image Registration; Landmark Detection; Pulmonary Diseases; Image Processing, Computer-Assisted; Anatomic Landmarks; Computed X Ray Tomography; Mathematical Concepts

1. Introduction

Accurate registration of lung CT images is a prerequisite for numerous clinical applications of medical image processing. Examples range from estimation of motion fields in 4DCT images for motion management during radiotherapy of lung tumors [1] over improved assessment of operation success or lung disease progression by registration of follow-up CT data [2] to enhanced diagnosis of emphysema or functional small-airways disease by registration-based analysis of a local volume change between end-inspiration/expiration lung CT scan pairs [3]. These applications led to a great interest in image registration of lung CT scans over the past years (e.g. [2], [4], [5], [6], [7], [8], [9], [10]), with most state-of-the-art approaches in this field being formulated as nonlinear intensity-based registration methods.

The accuracy of lung CT registration is commonly evaluated using corresponding anatomical landmarks identified within the images to be registered [2], [7], [8], [10]. Typical landmarks are bifurcations of bronchial and vessel trees and are usually annotated by human observers. Their identification, however, is time consuming and efforts have been made to automate the process [11], [12], [13]. The reported promising performance of these approaches motivates the integration of the automatically detected (sparse) correspondence information into intensity-based registration as additional knowledge.

Interpreting the automatically detected landmarks within the lungs as specific image features, their integration into intensity-based registration finally leads to hybrid feature- and intensity-based registration. Related work on the combination of intensity- and feature-based registration can be found in, e.g., [14], [15] , [16], [17], [18], [19], [20],; however, none of these papers tackles the problem of lung CT registration.

The contribution of this paper is twofold. First, a new pipeline for lung CT registration is introduced comprising of an automatic landmark detection algorithm [12] and a hybrid landmark- and intensity-based technique [21], [22]. The second contribution is a thorough quantitative evaluation and statistical testing of the underlying hypothesis that the combination of these two building blocks is more accurate than each approach solely used.

2. Methods

Following [23], image registration is concerned with finding a physically plausible transformation y that describes the correspondence between two given images. These images will be referred to as reference image R and template image T. It is well known that landmark detection methods can reliably and accurately establish this correspondence at certain distinctive points [11]. After sketching an algorithm specifically tailored for the problem of landmark detection and matching in lung CT scans, we will describe how to integrate this information into an intensity-based nonlinear registration method.

2.1. Automatic Landmark Detection

The applied approach for automatic detection of landmark correspondences between the images to be registered is based on [11] and [12]. The algorithm consists of two separate phases: identification of landmark candidates in the reference image R and transferring them to the template image T. The candidate identification in R is based on a

voxel-wise computation of a distinctiveness value. This value describes the similarity of a voxel to its neighbors [13] and is calculated as mean squared intensity difference to all surrounding voxels.

As we aim for the detection of anatomically characteristic points like bifurcations of vessels or bronchi, which are both characterized by high curvature, the distinctiveness value is scaled using an appropriate operator, see Figure 1. As proposed in [24], the Op3 operator is used for this purpose.

For the second phase, i.e. transferring the detected landmark candidates (voxels with high distinctiveness values) from R to T, a two-step correlation-based blockmatching strategy is exploited. The landmark candidates are first transferred by a common intensity-based blockmatching procedure. Then, they are additionally transferred by performing a second blockmatching run, this time based on the distinctiveness values computed for R and T. After both matching runs, plausibility checks are introduced to improve robustness of the transfer; cf. [12] for details.

2.2. Image Registration

For the three-dimensional scans considered here, let $R, T: \mathbb{R}^3 \supset \Omega \rightarrow \mathbb{R}$ denote reference and template image with compact domain Ω. Following the variational formulation described in [23], we compute the a priori unknown transformation $y: \mathbb{R}^3 \rightarrow \mathbb{R}^3$ that is used to obtain a modified template image $T(y)$, which is similar to R, by solving the following optimization problem:

$$\mathcal{J}(y) \coloneqq \mathcal{D}(y) + \alpha \mathcal{S}\big(y - y_{Ref}\big) = \text{min!} \tag{1}$$

The joint objective functional $\mathcal{J}$ consists of a distance measure $\mathcal{D}$ and a regularizer $\mathcal{S}$ favoring plausible transformations [23]. The regularization term is weighted by the parameter $\alpha \in \mathbb{R}^+$, which enables a balance between data fit (image distance) and deformation regularity. The reference transformation y_{Ref} is considered a plausible transformation (e.g. the result of a pre-registration) and is therefore not penalized.

As distance measure a variant of the Normalized Gradient Fields (NGF) [25] is used, which is well-suited for proper alignment of edges represented e.g. by vessels and bronchi in the lung CT data [4]:

$$\mathcal{D}(y) \coloneqq \int_{\Omega} 1 - \frac{\langle \nabla T\big(y(x)\big), \nabla R(x) \rangle_\eta^2}{\|\nabla T(y(x))\|_\eta^2 \|R(x)\|_\eta^2} \, dx \tag{2}$$

with $\langle a, b \rangle_\eta \coloneqq \eta^2 + \sum_{i=1}^3 a_i \, b_i$ and $\|a\|_\eta^2 \coloneqq \langle a, a \rangle_\eta$. The edge parameter $\eta \in \mathbb{R}^+$ allows for distinction between image features and noise-related edges. A major advantage of NGF is its independence of absolute intensity differences between corresponding areas in template and reference image as it was designed for multi-modal image registration. This feature pays off especially in registration of images acquired during different breathing phases. Here, intensity differences occur due to altered density of lung tissue and hence changed absorption of X-rays during acquisition of CT data.

Based on the findings in [4], curvature regularization [26] is employed:

$$\mathcal{S}(y) \coloneqq \sum_{i=1}^3 \int_{\Omega} \big(\Delta y_i(x)\big)^2 \, dx. \tag{3}$$

Potential breathing-induced sliding effects and possible discontinuities near the lung borders are accounted for by masking the images with lung segmentations, cf. [4]. Segmentations for the reference (Seg_R) and template images (Seg_T) are generated with the algorithm of Lassen et al. [27], which performed best in the LOLA11 challenge [28] for lung and lung lobe segmentation in chest CT scans.

A local minimizer of (1) is obtained in a Discretize-then-Optimize scheme using multilevel representations of the data. By solving the problem from coarse to fine, the risk of getting stuck in local minima during optimization is reduced and the multilevel approach acts as an additional regularizer. For numerical optimization of the discretized objective functional, the Gauss-Newton method combined with Armijo line search and a Conjugate Gradients solver was used, cf. [29]. The described registration scheme without usage of landmarks is subsequently called Multilevel Image Registration (MLIR) [23]. As an additional pre-registration step of MLIR, we employ an affine-linear registration of the lung masks.

2.3. Combining Landmarks and Distance Measures (CoLD)

For integration of the automatically detected landmark correspondences into the registration scheme MLIR described in the previous section, the so-called CoLD method is exploited. CoLD was introduced in [21] and later adjusted to the Discretize-then-Optimize scheme [22] used in this work. The fundamental idea of CoLD is to restrict the MLIR scheme to transformations that map the landmarks onto their corresponding locations in the other image. By formulating the approach as a constrained optimization problem, the combined registration can be achieved in one unified algorithm; see [22].

Assuming L landmark pairs (r_j, t_j), $j = 1, \dots, L$ have been established by the automatic landmark detection algorithm from section 2.1, the associated constrained optimization problem is given by:

$$\mathcal{J}(y) = \text{min! subject to } y(r_j) = t_j, \qquad j = 1, \dots, L. \tag{4}$$

In order to find a feasible starting point for the minimization of (4), i.e. a transformation fulfilling the landmark constraints, we employ a thin-plate spline (TPS) based transformation [24]. TPS transformations have been earlier used to successfully establish landmark correspondences in lung CT images; see, e.g., [13]. Furthermore, there exists a close relation to the applied curvature regularization approach [26], [30]. The calculated solution y_{TPS} maps each reference landmark r_j to its corresponding template landmark $t_j, j = 1, \dots, L$.

Following the CoLD approach, the sought transformation is decomposed as $y = y_{TPS} + y_h$. The homogenous solution y_h is chosen such that it does not interfere with the constraints of (4) but offers further degrees of freedom for the optimization of $\mathcal{J}$. For this purpose, a linear operator Z is constructed that maps a transformation v onto the homogenous solution $y_h = Z(v)$. For details on Z and the discretization of the described functions that are necessary for numerical optimization, we refer the reader to the description in [22].

With the help of Z it is possible to transform (4) into an unconstrained optimization problem. We set $y_{Ref} = y_{TPS}$ and obtain:

$$\mathcal{J}^{CoLD}(v) \coloneqq \mathcal{D}(y_{TPS} + Z(v)) + \alpha \mathcal{S}(Z(v)) = \text{min!} \tag{5}$$

The minimization problem (5) can now be solved analogously to (1) with a Gauss-Newton approach as described in Section 2.2. For further details on the discretization of distance measure and regularizer the interested reader is referred to [23].

3. Experiments and Results

3.1. Study Design and Data

The presented pipeline of automatic landmark detection and hybrid registration (originating from [21], [22]) is subsequently referred to as CoLD. To analyze the potential benefit of the combination of landmark and intensity information for the application of lung CT registration, we compare CoLD to the purely intensity-based registration approach of Section 2.2, referred to as MLIR, see [23], and the TPS transformation (described in [24]) as computed based on the automatically detected landmarks. The applied evaluation criteria are described in Section 3.2.

We chose ten data sets provided by the DIR-Lab ([5], [7]) as the basis for this comparison on pulmonary CT data. Together with the additionally provided landmarks they are a well-known publicly available benchmark database for lung CT registration. From each data set, the scan during maximal inspiration was chosen as reference and the maximal expiration scan as template image because in this scenario the largest motions occur, which makes the registration task more difficult. The axial resolution of the data varies from 0.97 mm × 0.97 mm to 1.16 mm × 1.16 mm and the resolution in inferior-superior direction is 2.5 mm for all data sets. Each data set contains 300 landmark pairs that were manually annotated by medical experts and are well distributed over the entire lung volume [5], [7]. Note that these landmarks were exclusively used for evaluation of registration accuracy, but not as input to TPS and CoLD.

The generated lung segmentations were used to extract the lung volumes from the scans, on which registrations were performed. As second preprocessing step, data sets 6 to 10 were cropped by removing voxels that do not belong to a bounding box of the lung segmentations plus a margin of five voxels to avoid artifacts at the boundaries. Each data set was finally resampled to a maximal resolution of $\mathbf{m}$ = (256, 256, 128) to reduce the computational demands.

The multi-level pyramid used for registration consisted of five levels, i.e. we started with a discretization of $\mathbf{m}_0 = (16,16,8)$ as a compromise between speed and valuable information necessary for intensity-based registration. The parameters $\alpha = 4$ and $\eta = 150$ were determined empirically and used for MLIR as well as for CoLD on all data sets. All implementations were done in MATLAB® based on the FAIR registration toolbox [23].

3.2. Evaluation Criteria

Computing the distance of expert-annotated landmarks after registration is a common procedure for evaluation of the accuracy of registration methods, cf. e.g., [2], [8]. Let $d_{i,j} = ||y(r_j^i) - t_j^i||\,, i = 1, \dots, 10, j = 1, \dots, 300$ denote the Euclidean distance of transformed reference and template landmark number j in data set number i. Following [5], [6], [7], we report mean values and standard deviations of the distances per data set. As these Euclidean distances are not necessarily normally distributed, we employed one-sided Wilcoxon rank sum tests for significance testing of the landmark distance reduction between the registration algorithms. Median landmark distances on data set i are denoted as $\tilde{d}_i$, mean values as $\bar{d}_i$, standard deviations as σ_i and maximum distances as M_i. The three tested null

hypotheses for data set i were: $\tilde{d}_i^{\mathrm{TPS}} \leq \tilde{d}_i^{\mathrm{CoLD}}$, $\tilde{d}_i^{\mathrm{MLIR}} \leq \tilde{d}_i^{\mathrm{CoLD}}$ and $\tilde{d}_i^{\mathrm{MLIR}} \leq \tilde{d}_i^{\mathrm{TPS}}$. The considered Bonferroni corrected significance level was $\alpha = \frac{0.05}{3}$.

As we aim for an evaluation of the entire deformation field while the landmarks are located at only a few positions, we also analyzed the Jacobian determinant $|\nabla y(x)|$ of the transformation y. The Jacobian measures the local volume change: A value of $|\nabla y(x)| = 1$ means volume preservation, a deviation from 1 indicates local volume expansion ($|\nabla y(x)| > 1$) or contraction ($|\nabla y(x)| < 1$). If $|\nabla y(x)| > 0$, the deformation is invertible at x [31]. If $|\nabla y(x)| < 0$ a change of orientation occurred. Hence, we consider values $|\nabla y(x)| \leq 0$ as implausible singularities for a lung deformation [2]. Moreover, the average Jacobian determinant value over all lung voxels should correlate with the ratio of template lung volume to reference lung volume. This indicates a good global alignment as this ratio is an estimator for the volume change of the whole lung tissue.

3.3. Results

Figure 2 shows registration results as absolute difference of reference and transformed template image. Visual inspection of Figure 2 (c) and (g) indicates a good alignment of large vessels and lung boundaries by the purely landmark-based TPS solution. Although MLIR gives satisfying results in (b), it fails to register properly for the 8$^{\text{th}}$ case (Figure 2 (f)) as many vessels of reference and template image are not aligned and have high intensity differences, i.e., they are bright. In total, results of CoLD ((d) and (h)) give the best visual impression.

Quantitative registration results concerning landmark distances for the three tested methods and the initial situation are summarized in Table 1. The observer error is integrated to show the distances that medical experts can achieve when performing manual propagation of the reference landmarks to the template image. The values are considered as lower boundary for the achievable registration accuracy. As the manual landmark annotations from [5], [7] were restricted to the voxel grid, the deformed reference landmark positions were moved to the closest voxel center before computing the Euclidean landmark distances (see also [2]). The values show that the proposed hybrid registration approach CoLD clearly outperforms both the TPS and the MLIR method; CoLD achieves a mean landmark distance of 1.15 mm over all data sets (TPS: 1.68 mm; MLIR: 2.44 mm). CoLD consistently produced the lowest mean and median landmark distances in all ten cases. In eight out of these ten cases a significant difference in median distance to TPS is given by one-sided Wilcoxon rank sum tests. For the comparison of MLIR and CoLD, a significant result in favor of CoLD is achieved on nine of ten data sets. The detailed results are given in Table 2.

The results of the Jacobian determinant analysis are summarized in Table 3. The analysis of $|\nabla y(x)|$ reveals plausible minimal and maximal values for all registration approaches. None of the methods produces singularities. Furthermore, the minimal contraction to approximately half the volume in most cases is within our expectations. The maximal values are in a realistic range as at most a local expansion of 63 % occurs. The global volume change ($|\mathrm{Seg}_T| \,/ |\mathrm{Seg}_R|$) is also approximated well by all three algorithms with the best method for this criterion again being CoLD.

The landmark detection algorithm computed at least 137 (data set 6), on average 239 and at most 375 (data set 2) landmark pairs. A qualitative result concerning spatial landmark distribution is given for data set 1 in Figure 1.

4. Discussion and Conclusions

We have presented a combination of automatic detection of landmark correspondences in lung CT images and a nonlinear intensity-based registration. Comparison with a traditional nonlinear intensity-based and a landmark-based TPS registration reveals that the proposed combined approach outperforms both its building blocks if applied as individual components. Hence, the combination of landmark and intensity information is valuable for the important problem of lung CT registration.

In general, the quality of the landmark correspondences established by the landmark detection algorithm was very high, which is reflected by good results after registration with the TPS method that exclusively takes the landmark pairs as input. As the number of landmark pairs was rather low (239 on average) compared to the mean number that was originally set by the medical experts (on average 882 [5], [7], only 300 landmarks per data set are publically available), there should still be potential for further improvement concerning both the number of the detected landmark candidates and especially the robustness of their transfer from reference to template image. As future work, we plan to address this issue by using multi-level and multi-scale techniques as well as further local refinements of the landmark matching.

On the registration side, the inherent CoLD assumption that landmarks can be unambiguously assigned to their corresponding locations is under debate [16]. Preliminary work using tolerances for the landmark assignment [32] shows very promising results. Hence, the systematic comparison of different ways of combining landmarks and intensity information for the problem of CT lung registration is subject to future investigation.

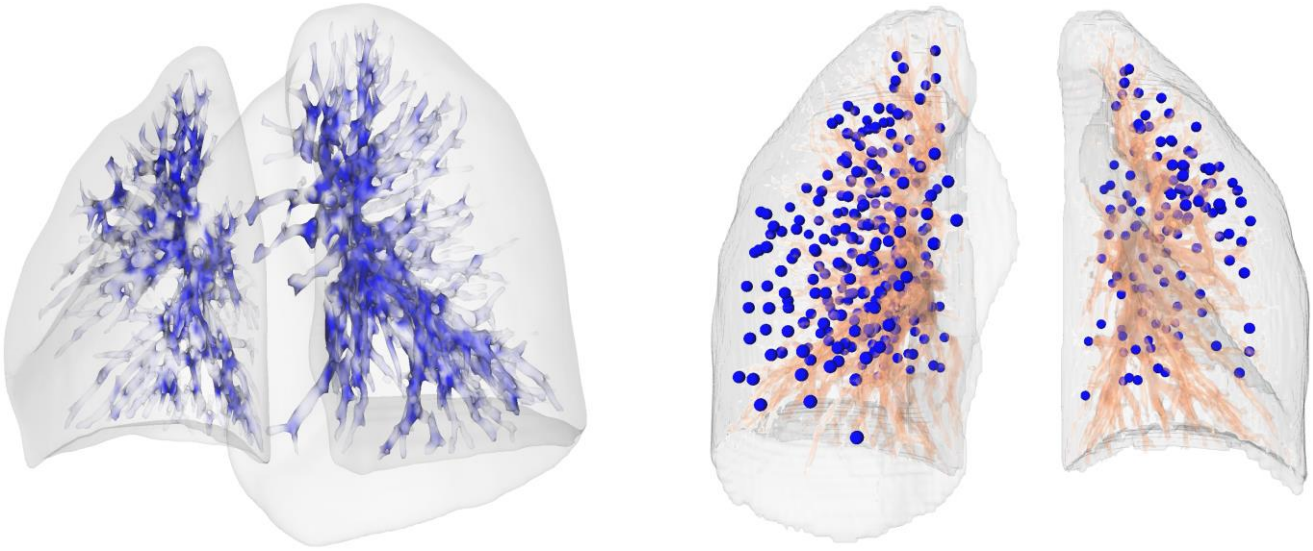

Figure 1: Visualization of landmark detection. Left: Op3 operator answers. High values correspond to dark blue colors. Right: Detected landmarks are shown as dots.

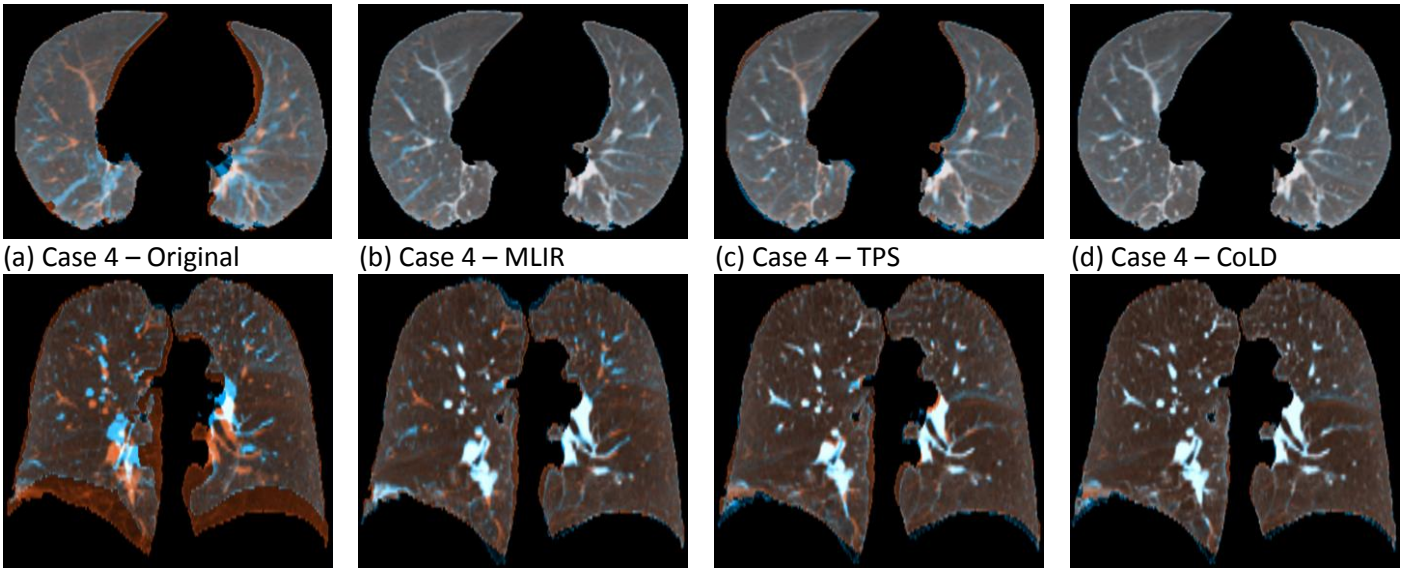

(a) Case 4 – Original (b) Case 4 – MLIR (c) Case 4 – TPS (d) Case 4 – CoLD

(e) Case 8 – Original (f) Case 8 – MLIR (g) Case 8 – TPS (h) Case 8 – CoLD

Figure 2: Overlay of reference (orange) and (transformed) template image (blue) in an axial view of the 4th case (top row) and in a coronal view of the 8th case (bottom row). Correctly aligned structures are grey or white.

Table 1: Statistics of distances of DIR-Lab landmarks for the three tested methods after registration. Second column shows mean (standard deviation) observer errors of medical experts of the DIR-Lab ([5], [7]). Columns labeled as "initial" report distances without registration. All values are given in mm; best results are printed bold.

Case (i)	Observer Error	Mean ($\bar{d}_i$)				Standard deviation (σ_i)				Maximum (M_i)			
		Initial	TPS	MLIR	CoLD	Initial	TPS	MLIR	CoLD	Initial	TPS	MLIR	CoLD
1	0.85 (1.24)	3.89	0.94	1.08	**0.79**	2.78	1.07	1.05	**0.93**	10.90	5.00	3.71	**3.31**
2	0.70 (0.99)	4.34	0.91	1.04	**0.79**	3.90	0.96	1.19	**0.93**	17.69	**3.60**	4.87	**3.60**
3	0.77 (1.01)	6.94	1.21	1.93	**0.90**	4.05	1.22	1.80	**1.11**	16.55	**6.07**	10.26	6.79
4	1.13 (1.27)	9.83	1.94	2.12	**1.37**	4.86	1.52	2.17	**1.19**	20.25	11.75	14.84	**10.17**
5	0.92 (1.16)	7.48	1.86	1.94	**1.44**	5.51	**1.60**	1.96	**1.60**	24.78	**15.39**	16.60	16.60
6	0.97 (1.38)	10.89	1.98	1.89	**1.06**	6.97	1.65	1.60	**1.23**	27.59	12.13	**6.70**	8.50
7	0.81 (1.32)	11.03	2.14	3.08	**1.29**	7.43	1.51	2.31	**1.27**	30.64	8.04	10.19	**6.48**
8	1.03 (2.19)	14.99	2.16	5.08	**1.45**	9.01	1.50	4.22	**1.40**	30.57	**9.74**	20.38	10.41
9	0.75 (1.09)	7.92	1.85	3.35	**1.20**	3.98	1.22	2.71	**1.06**	15.76	5.87	11.93	**5.36**
10	0.86 (1.45)	7.30	1.80	2.87	**1.24**	6.35	1.60	2.79	**1.56**	27.79	**11.51**	12.87	11.55
Average	0.88 (1.31)	8.46	1.68	2.44	**1.15**	5.48	1.39	2.18	**1.23**	22.25	8.91	11.23	**8.28**

Table 2: Results (p-values) of one-sided Wilcoxon rank sum test. Null hypothesis is that median of 1st method is less or equal than median of 2nd method. Significant results ($p < \frac{0.05}{3} \approx 0.0167$) are bold.

Case (i)	1	2	3	4	5	6	7	8	9	10
TPS vs. CoLD	0.1091	0.0700	**0.0010**	$< \mathbf{10^{-6}}$	$< \mathbf{10^{-4}}$	$< \mathbf{10^{-9}}$	$< \mathbf{10^{-9}}$	$< \mathbf{10^{-9}}$	$< \mathbf{10^{-9}}$	$< \mathbf{10^{-8}}$
MLIR vs. CoLD	**0.0004**	0.0216	$< \mathbf{10^{-9}}$	$< \mathbf{10^{-4}}$	**0.0004**	$< \mathbf{10^{-9}}$	$< \mathbf{10^{-9}}$	$< \mathbf{10^{-9}}$	$< \mathbf{10^{-9}}$	$< \mathbf{10^{-9}}$
MLIR vs. TPS	0.0281	0.2587	$< \mathbf{10^{-5}}$	0.7543	0.7055	0.8670	$< \mathbf{10^{-6}}$	$< \mathbf{10^{-9}}$	$< \mathbf{10^{-9}}$	$< \mathbf{10^{-4}}$

Table 3: Statistics on Jacobian determinants $|\nabla y(x)|$. The second column equals the template image lung volume divided by reference image lung volume. The values for the method that approximates this ratio best are bold.

Case	$\frac{\lvert \mathrm{Seg}_T \rvert}{\lvert \mathrm{Seg}_R \rvert}$	Average			Minimum			Maximum		
		TPS	MLIR	CoLD	TPS	MLIR	CoLD	TPS	MLIR	CoLD
1	0.915	0.931	0.920	**0.917**	0.555	0.639	0.547	1.167	1.355	1.277
2	0.917	0.927	0.925	**0.919**	0.708	0.577	0.641	1.132	1.216	1.299
3	0.896	0.914	0.904	**0.896**	0.633	0.608	0.616	1.205	1.571	1.628
4	0.861	**0.859**	**0.863**	0.843	0.525	0.535	0.475	1.202	1.333	1.367
5	0.905	0.895	0.909	**0.902**	0.517	0.505	0.478	1.212	1.254	1.308
6	0.770	0.826	**0.776**	0.777	0.552	0.412	0.149	1.114	1.239	1.228
7	0.812	0.837	0.826	**0.817**	0.642	0.488	0.520	1.022	1.248	1.219
8	0.830	0.847	0.837	**0.834**	0.523	0.487	0.488	1.087	1.315	1.351
9	0.859	0.894	0.860	**0.859**	0.614	0.557	0.506	1.260	1.250	1.395
10	0.859	0.881	0.869	**0.854**	0.504	0.563	0.459	1.084	1.383	1.360

References

[1] Wang H, Dong L, O'Daniel J, Mohan R, Garden AS, Ang KK, et al. Validation of an Accelerated 'Demons' Algorithm for Deformable Image Registration in Radiation Therapy. Phys Med Biol. 2005;50:2887-905.

[2] Murphy K, van Ginneken B, Reinhardt JM, Kabus S, Ding K, Deng X, et al. Evaluation of Registration Methods on Thoracic CT: the EMPIRE10 Challenge. IEEE T Med Imaging. 2011;30:1901-20.

[3] Galbán CJ, Han MK, Boes JL, Chughtai KA, Meyer CR, Johnson TD, et al. Computed Tomography-based Biomarker Provides Unique Signature for Diagnosis of COPD Phenotypes and Disease Progression. Nat Med. 2012;18:1711-15.

[4] Rühaak J, Heldmann S, Kipshagen T, Fischer B. Highly Accurate Fast Lung CT Registration. In: Ourselin S, Haynor DR, editors. SPIE Medical Imaging 2013: Image Processing. Proceedings of SPIE Volume 8669; 2013 Feb 9-14; Lake Buena Vista, Florida, USA. p. 86690Y-1-9.

[5] Castillo E, Castillo R, Martinez J, Shenoy M, Guerrero T. Four-dimensional Deformable Image Registration using Trajectory Modeling. Phys Med Biol. 2010;55:305-27.

[6] Castillo E, Castillo R, White B, Rojo J, Guerrero T. Least Median of Squares Filtering of Locally Optimal Point Matches for Compressible Flow Image Registration. Phys Med Biol. 2012;57:4827-33.

[7] Castillo R, Castillo E, Guerra R, Johnson VE, McPhail T, Garg AK, et al. A Framework for Evaluation of Deformable Image Registration Spatial Accuracy using Large Landmark Point Sets. Phys Med Biol. 2009;54:1849-70.

[8] Kabus S, Klinder T, Murphy K, van Ginneken B, Lorenz C, Pluim JPW. Evaluation of 4D-CT Lung Registration. In: Yang GZ, Hawkes D, Rueckert D, Noble A, Taylor C, editors. MICCAI 2009: Proceedings of the 12th International Conference on Medical Image Computing and Computer-Assisted Intervention; 2009 Sep 20-24; London, UK. Berlin: Springer LNCS vol. 5761 p. 747-54.

[9] Schmidt-Richberg A, Werner R, Ehrhardt J, Wolf JC, Handels H. Landmark-driven Parameter Optimization for Non-linear Image Registration. In: Dawant BM, Haynor DR. SPIE Medical Imaging 2011: Image Processing. Proceedings of SPIE Volume 7962; 2011 Feb 12-17; Lake Buena Vista, Florida, USA. p. 0T1-8.

[10] Riyahi-Alam S, Peroni M, Baroni G, Riboldi M. Regularization in Deformable Registration of Biomedical Images Based on Divergence and Curl Operators. Methods Inf Med. 2014;53:21-28.

[11] Likar B, Pernuš F. Automatic Extraction of Corresponding Points for the Registration of Medical Images. Med Phys. 1999;26:1678-86.

[12] Werner R, Duscha C, Schmidt-Richberg A, Ehrhardt J, Handels H. Assessing Accuracy of Non-linear Registration in 4D Image Data using Automatically Detected Landmark Correspondences. SPIE Medical Imaging 2013: Image Processing. Proceedings of SPIE Volume 8669; 2013 Feb 9-14; Lake Buena Vista, Florida, USA.

[13] Murphy K, van Ginneken B, Klein S, Staring M, de Hoop, BJ, Viergever MA, et al. Semi-automatic Construction of Reference Standards for Evaluation of Image Registration. Med Image Anal. 2011;15:71-84.

[14] Olesch J, Papenberg N, Lange T, Conrad M, Fischer B. Matching CT and Ultrasound Data of the Liver by Landmark Constrained Image Registration. In: Miga MI, Wong, KH. SPIE Medical Imaging 2009: Visualization, Image-Guided Procedures, and Modeling. Proceedings of SPIE Volume 7261; 2009 Feb 8-12; Lake Buena Vista, Florida, USA. p. 72610G1-7.
[15] Papenberg N, Olesch J, Lange J, Schlag PM, Fischer B. Landmark Constrained Non-parametric Image Registration with Isotropic Tolerances. In: Meinzer HP, Deserno TM, Handels H, Tolxdorff T, editors. BVM 2009: Proceedings of the 12th Workshop on Bildverarbeitung für die Medizin. 2009 Mar 22- 25; Heidelberg, Germany. Berlin: Springer; 2009 p. 122-6.
[16] Lange T, Papenberg N, Olesch J, Fischer B, Schlag PM. Landmark Constrained Non-rigid Image Registration with Anisotropic Tolerances. In: Dössel O, Schlegel WC, editors. World Congress on Medical Physics and Biomedical Engineering. 2009 Sep 7-12; Munich, Germany. Berlin: Springer IFMBE Proceedings vol. 25/4 p. 2238–41.
[17] Hellier P, Barillot, C. Coupling Dense and Landmark-Based Approaches for Nonrigid Registration. IEEE T Med Imaging. 2003;22:217-27.
[18] Johnson HJ, Christensen GE. Consistent Landmark and Intensity-based Image Registration. IEEE T Med Imaging. 2002;21:450-61.
[19] Kybic J, Unser M. Fast Parametric Elastic Image Registration. IEEE T Image Process. 2003;12:1427-42.
[20] Papademetris X, Jackowski AP, Schultz RT, Staib LH, Duncan JS. Integrated Intensity and Point-Feature Nonrigid Registration. In: Barillot C, Haynor D, Hellier P. MICCAI 2004: Proceedings of the 7th International Conference on Medical Image Computing and Computer-Assisted Intervention; 2004 Sep 26-29; Saint-Malo, France. Berlin: Springer LNCS vol. 3216 p. 763-70.
[21] Fischer B, Modersitzki J. Combining Landmark and Intensity Driven Registrations. Proc Appl Math Mech. 2003; 3:32-5.
[22] Haber E, Heldmann S, Modersitzki J. A Scale-Space Approach to Landmark Constrained Image Registration. In: Tai XC, Morken K, Lysaker M, Lie KA. SSVM 2009: Proceedings of the 2nd International Conference on Scale Space Methods and Variational Methods in Computer Vision;2009 Jun 1-5; Voss, Norway. p. 612-23. Springer LNCS vol. 5567.
[23] Modersitzki J. FAIR: Flexible Algorithms for Image Registration. Philadelphia: SIAM; 2009.
[24] Rohr K. Landmark-based Image Analysis. Norwell, MA, USA: Kluwer Academic Publishers; 2001.
[25] Haber E, Modersitzki J. Intensity Gradient Based Registration and Fusion of Multi-modal Images. Methods Inf Med. 2007;46:292-9.
[26] Fischer B, Modersitzki J. Curvature Based Image Registration. J Math Imaging Vis. 2003;18:81-5.
[27] Lassen B, Kuhnigk JM, Schmidt M, Krass S, Peitgen HO. Lung and Lung Lobe Segmentation Methods at Fraunhofer MEVIS. In: Beichel RR, de Bruijne M, van Ginneken B, Kabus S, Kiraly AP, Kuhnigk JM, et al. Proceedings of the 4th International Workshop on Pulmonary Image Analysis; 2011 Sep 18; Toronto, Canada. p. 185–99.
[28] Lola11.com [Internet]. LObe and Lung Analysis 2011 [cited 2014 Mar 7], Available from: http://lola11.com/Results/Overview.
[29] Nocedal J, Wright SJ. Numerical Optimization. 2nd ed. New York: Springer; 2006.
[30] Modersitzki J. Numerical Methods for Image Registration. New York: Oxford University Press; 2004.
[31] Ciarlet PG. Mathematical Elasticity. New York: North-Holland;1988.
[32] Polzin T, Rühaak J, Werner R, Strehlow J, Heldmann S, Handels H, Modersitzki J. Combining Automatic Landmark Detection and Variational Methods for Lung CT Registration. In: Beichel RR, de Bruijne M, Kabus S, Kiraly AP, Kuhnigk JM, et al. Proceedings of the 5th International Workshop on Pulmonary Image Analysis; 2013 Sep 26; Nagoya, Japan. p. 85-96.